Accepted for publication in Journal of Magnetic Resonance

DOI: 10.1016/j.jmr.2021.107081

A 2.0-GHz compact ESR spectrometer for monitoring automobile lubrication oil degradation

Fan Cheng,[a,*] Takayuki Shibata,[a] Yoshifumi Aoki,[b] Hiroshi Hirata[c]

[a] Sensor Research & Development Division, MIRISE Technologies Corporation, 500-1 Minamiyama, Komenoki-cho, Nisshin, Aichi, 470-0111, Japan

[b] TOYOTA CENTRAL R&D LABS., INC., 41-1, Yokomichi, Nagakute, Aichi, 480-1192, Japan

[c] Division of Bioengineering and Bioinformatics, Faculty of Information Science and Technology, Hokkaido University, North 14, West 9, Kita-ku, Sapporo, 060-0814, Japan

* Corresponding author:

Fan Cheng
Sensor Research & Development Division
MIRISE Technologies Corporation
500-1 Minamiyama, Komenoki-cho
Nisshin, Aichi, 470-0111, Japan
Phone: +81-561-75-1069
E-mail: han.tei.j6z@mirise-techs.com

Abstract

This article reports a simple, compact, and cost-effective electron spin resonance (ESR) spectrometer for monitoring automobile lubrication oil degradation. Lubrication oil degradation strongly correlates with the concentration of stable free radicals caused by hydrocarbon chain decomposition due to heating. For the prototype spectrometer, the amplitude shift in a marginal oscillator output detects ESR absorption in a sample. The spectrometer's spin sensitivity of 2.3×10^{14} spins for a used oil sample was achieved using the marginal oscillator with a loop-gap resonator. For the prototype spectrometer, the oscillation frequency was 2.09 GHz. The volume of the prototype spectrometer was 1.3 L, including a permanent magnet, microwave circuits, and digital communication circuitry on printed circuit boards. The weight of the spectrometer setup was 1.45 kg. This prototype spectrometer successfully detected the ESR signal from a 50 μL oil sample (spin concentration 8.3×10^{19} spins/L) with a signal-to-noise ratio of 37 and an acquisition time of 30 s.

Keywords: Lubrication oil, marginal oscillator, compact ESR spectrometer, loop-gap resonator

Highlights:

- A 2.0-GHz ESR spectrometer was developed to detect lubrication oil degradation.
- The prototype spectrometer is compact for use in the automobile industry.
- A marginal oscillator can help detect ESR absorption at 2.0 GHz.
- The oscillator circuit involves a loop-gap resonator to realize oscillation.

Graphical Abstract

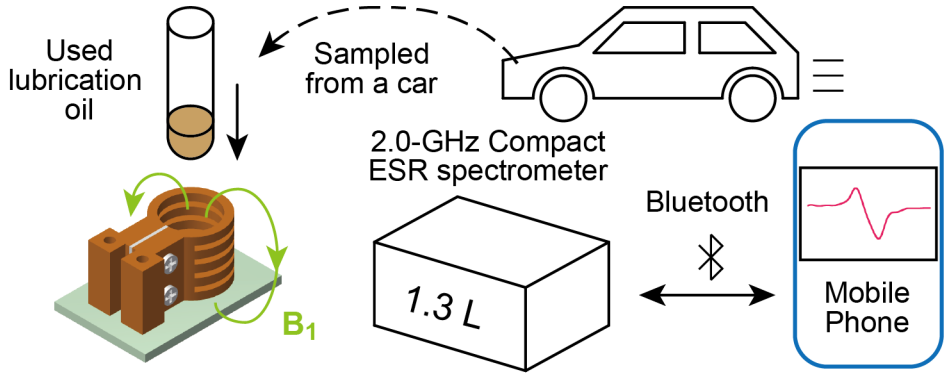

1. Introduction

Lubrication oil is essential to reduce friction in machinery in all industries and in daily life. The estimated worldwide demand for lubrication oil was 11.8 billion gallons per year in 2017 [1]. In 2018, automotive fluids accounted for 48% of the total demand for lubrication oil in the United States of America [1]. Such oil consumption is an important concern in environmental protection even with appropriate oil waste disposal. Moreover, deteriorated lubrication oil increases engine-related problems and the need for automobile maintenance. Therefore, the assessment of its degradation and its maintenance are crucial to prolonging an automobile's lifetime and keeping lubrication oil in good condition.

These concerns require the ability to assess lubrication oil degradation. Conventional systems for sensing oil degradation use pH [2, 3], optical properties [4–9], electrical impedance [9–16], and viscosity [17–22] in addition to visual inspection and evaluation by feel. However, no scientifically reliable method is used daily in the automobile industry, such as at gas stations. Oil oxidation is a major reason for oil degradation and is caused by the chain decomposition of hydrocarbons due to heating. In this process, free radicals are generated in oil as a by-product [1, 2, 23, 24]. The number of stable free radicals is strongly correlated with the degradation of lubrication oil caused by the breakdown of lubricant molecules [25]. Electron spin resonance (ESR) spectroscopy is a powerful tool for detecting free radicals to monitor the degradation of lubrication oil. Therefore, ESR spectroscopy may be used to suggest an appropriate maintenance schedule for lubrication oil in a vehicle engine.

However, a commercially available laboratory-use ESR spectrometer is large and expensive. Low cost and ease of operation are crucial for its use at general car

service stations or gas station. An ESR spectrometer for monitoring the degradation of lubrication oil would require the following features: (i) a compact and portable design so that it could be used outside the laboratory, e.g., at a gas station; (ii) the minimum ESR detection sensitivity would need to be on the order of 10^{18} spins/L (this spin concentration for lubrication oil corresponds to a driving distance of approximately 1000 km in a previous report [25]); and (iii) the spectrometer should be able to indicate the appropriate timing to replace lubrication oil from the peak-to-peak signal intensity of the ESR spectrum. To fulfill the need for ESR-based oil degradation assessment, a compact and cost-effective ESR spectrometer could be a practical and useful tool for automobile maintenance. A simple microwave circuit and a compact magnet contribute to this spectrometer. Moreover, spin sensitivity is an essential component in the spectrometer design. Thus, the real challenge in developing such a spectrometer is to achieve a reasonable ESR detection sensitivity with a simple microwave circuit and a compact magnet.

A marginal oscillator is an excellent choice for building a simple microwave circuit, instead of the commonly used reflection-type homodyne detection scheme. This concept simplifies the microwave circuits for the spectrometer. Self-oscillating ESR spectrometers, which combine a cavity resonator with a Gunn diode, have been known since the 1970s [26–32]. These spectrometers do not use an automatic frequency control (AFC) system. However, since the Gunn diode should be integrated with the resonator, the Gunn diode must be insensitive to the applied magnetic field. Thus, the lack of non-magnetic high-frequency electronic components is crucial for self-oscillating ESR spectrometers.

Recently, chip ESR detectors that are based on the miniaturization of semiconductors have been reported [33–38]. An LC-circuit on a semiconductor chip

was used as an ESR resonator. Chip ESR detectors can measure a tiny sample (nano- or pico-liter scale). However, since used lubrication oil is abundant in automobiles, the sample availability for this application is not as limited as in the case of protein samples or nanoscale crystals. Therefore, ESR detectors that are made using the fabrication technologies of semiconductors are not necessarily required for measuring lubrication oil degradation. Sato-Akaba et al. reported a field-programmable gate array (FPGA)-based ESR spectrometer using the reflection-type homodyne detection scheme [39]. It used direct sampling of the radiofrequency (RF) signals reflected from the resonator, and all digital signal processing was performed in FPGA integrated circuits [39–41]. Modern FPGA technology in the ESR instrument is a possible approach to make the spectrometer setup compact. However, self-oscillating circuitry based on FPGA has not yet been explored for the ESR spectrometer.

For lubrication oil measurements, White et al. reported a benchtop and online Micro-ESR spectrometer in 2010 [42]. This spectrometer used a magnetic field of 115 mT and a microwave frequency of 3.4 GHz. Its dimensions and weight were 11.25 x 10 x 10 inches (286 mm x 254 mm x 254 mm) and 3 kg, respectively. In addition, several compact X-band EPR spectrometers are commercially available. For example, their dimensions and weights are 47 cm × 38 cm × 26 cm and 45 kg for Adani SPINSCAN X, 30.5 cm × 30.5 cm × 30.5 cm and 10 kg for Bruker microESR, and 39.7 cm × 26.2 cm × 19.2 cm and 45 kg for Bruker Magnettech ESR5000. Further miniaturization of the spectrometer and reducing its weight facilitate ESR spectroscopy for monitoring lubrication oil degradation in car service. Selection of the magnetic field strength and the corresponding microwave frequency is crucial to miniaturize the spectrometer. When the dimensions of the sample and the resonator

are constant, the signal-to-noise ratio (SNR) of an ESR spectrum at a constant microwave power is proportional to $\omega^{3/2}$, where ω is the microwave angular frequency [43]. Therefore, the spectrometer's detection sensitivity and downsizing (mainly the magnet size) by reducing the magnetic field strength is a trade-off. The ESR spectrometer design should balance the detection sensitivity, the spectrometer's dimensions, and weight. Such a spectrometer for monitoring oil degradation would be useful for the current automobile industry.

This article reports the development of a compact ESR spectrometer for monitoring the degradation of engine lubrication oil. To build this miniaturized spectrometer, we propose a spectrometer that uses a 2.0-GHz marginal oscillator, a loop-gap resonator (LGR), and a high electron mobility transistor (HEMT). The development of a resonator-integrated oscillator that is highly sensitive to ESR absorption is an engineering advancement in the present study. To demonstrate the assessment of oil degradation, we performed ESR spectroscopy for used lubrication oil with our compact spectrometer. The prototype ESR spectrometer achieved a detection sensitivity limitation of 2.3 x 10^{14} spins under the conditions of the peak-to-peak first-derivative ESR absorption linewidth of 1.0 mT and SNR = 2. The prototype spectrometer provided the required sensitivity for oil degradation detection. ESR spectroscopic data could suggest oil replacement at the appropriate timing with an analytical measure of free radical contents in passenger car lubrication oil in the future.

2. Materials and Methods

2.1. Design and configuration of a 2.0-GHz compact ESR spectrometer

Figure 1 illustrates the block diagram of a prototype 2.0-GHz compact continuous-wave (CW)-ESR spectrometer. The notable feature of this spectrometer is a marginal oscillator in conjunction with the LGR to simplify the microwave circuits of ESR detection. The spectrometer setup consists of four parts: (i) a permanent magnet and modulation coils, (ii) an oscillator circuit and an LGR, (iii) analog signal processing circuits, and (iv) a power supply and intermediate frequency (IF) circuits.

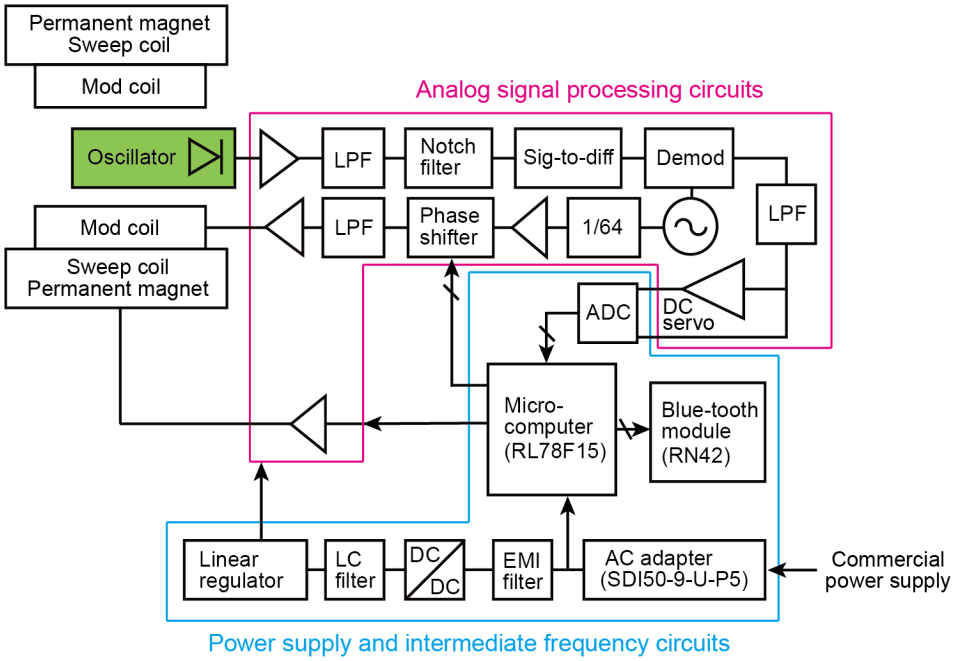

Fig. 1. Block diagram of the prototype ESR spectrometer system. The system consists of four units, i.e., (i) a permanent magnet and modulation coils, (ii) an oscillator circuit and an LGR, (iii) analog signal processing circuits, and (iv) a power supply and intermediate frequency (IF) circuits. Sig-to-diff, single-ended-to-differential signal conversion circuit; Demod, demodulator circuit; ADC, analog-to-digital converter; LPF, low-pass-filter; EMI, electromagnetic interference. Detailed circuit diagrams of analog signal processing circuits are given in the Supplementary Material (Figs. S1, S2, and S3).

We selected the magnetic field and a microwave frequency for electron spin excitation to make the spectrometer compact and potentially mobile. A higher

magnetic field gives a larger Zeeman energy splitting and a stronger ESR absorption signal than a lower magnetic field. However, a higher magnetic field generally requires a large permanent magnet than a lower magnetic field, and this is contrary to our aim to develop a compact ESR spectrometer. A magnetic field of 68.3 mT was available using a dedicated permanent magnet with a 40 mm x 50 mm footprint. Due to the compromise between the magnet size and the magnetic field, we used 68.3 mT as the minimum field strength. We also decided to use a microwave frequency of approximately 2.0 GHz for ESR spectroscopy (the corresponding central magnetic field is 71 mT when *g*-factor = 2.0). The details of each part of the spectrometer setup are described below.

2.2. Resonator

The LGR has two benefits for our spectrometer. First, the LGR contributes to miniaturization of the ESR spectrometer. The LGR is a lumped resonant structure; therefore, the diameter of the LGR is flexible for the microwave frequency we used [44, 45]. An LGR with a smaller diameter led to a decrease in the gap of the magnetic pole caps and a further reduction of the magnet size even to maintain the same magnetic field strength. Second, since the LGR has a higher filling factor, the LGR contributes to the ESR spectrometer's improvement in sensitivity. To enhance the sensitivity, we designed the LGR to fit for the 5-mm sample tube. Hence, the inner diameter of the LGR was set to 5.2 mm.

The LGR was fabricated using a wire electrical discharge machining (EDM) process of a high-purity copper plate. Figure 2A shows a photograph of the fabricated LGR. The LGR was based on single-turn loop coils and a capacitor with a dielectric substrate. High-purity copper with low conduction loss was used to obtain a

higher Q-factor. Cross-linked polystyrene (Rexolite® 1422, dielectric constant ε_r = 2.53) was chosen as a dielectric substrate because of its low dielectric loss to achieve a higher Q-factor of the capacitor.

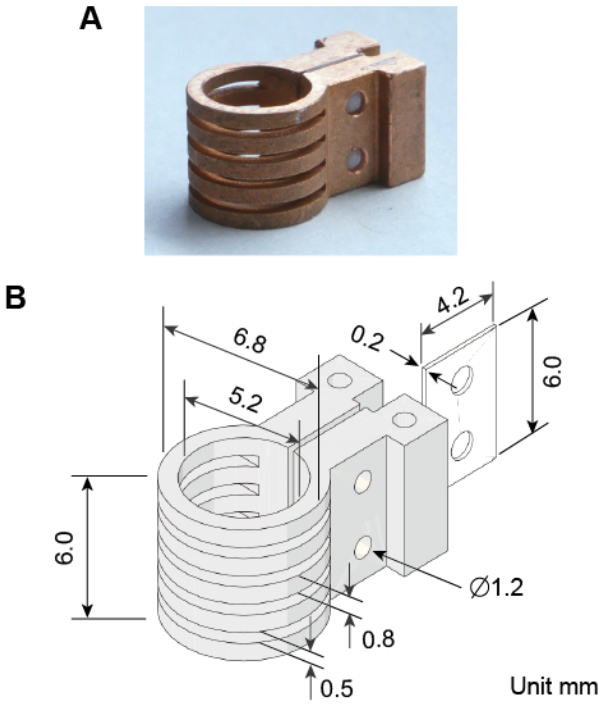

Fig. 2. Design and fabrication of a loop-gap resonator with a resonant frequency of 2.0 GHz. (A) Photograph of the developed LGR and (B) the dimensions of the LGR and a dielectric substrate for the gap. The conductive element was made of copper. The dielectric substrate was made of cross-linked polystyrene (Rexolite® 1422) and placed in the gap.

Figure 2B shows the dimensions of the resonator. The inner diameter, outer diameter, and height of the LGR were 5.2 mm, 6.8 mm, and 6.0 mm, respectively, to accommodate a typical ESR sample tube with a 5.0-mm diameter. In the conductive loop, parallel slits (0.5 mm in width) were made to decrease eddy currents due to the time-varying magnetic field, i.e., magnetic field modulation. The required sample

volume was 75 μL to fulfill the sample volume in the tube (6.0-mm height and 4.0-mm inner diameter). The capacitive gap dimensions were considered with the given inductive loops to adjust the LGR's resonant frequency. The dimensions of the dielectric substrate were 4.2 mm x 6.0 mm x 0.2 mm. The dielectric substrate was fixed in the gap with plastic screws.

2.3. Microwave Oscillator

The resonator-integrated oscillator design was based on a crystal oscillator, which used a piezoelectric transducer's mechanical resonance. This circuit configuration is also known as the Colpitts circuit. The LC tank circuit's resonant frequency determines the oscillation condition [46]. Under such a condition, the oscillation frequency changes with the inductive impedance of the excited resonator. For a crystal oscillator, the resonator's inductive impedance is necessary for the frequency band close to the natural frequency to satisfy the oscillation condition.

In contrast to the crystal oscillator, the inductively coupled LGR has a capacitive impedance near its resonant frequency. A quarter-wavelength transmission line was inserted between the coupling loop and the HEMT to satisfy the oscillation condition by converting the capacitive impedance of the LGR to an inductive impedance. Furthermore, the transmission line kept the HEMT and other electronic components of the oscillator away from the magnetic field.

The oscillation frequency was locked to the LGR's resonant frequency in the marginal oscillator. The oscillation frequency close to the LGR's resonance peak was essential to obtain a high ESR detection sensitivity. While AFC was required in the standard reflection-type CW-ESR spectrometer, it was unnecessary in the marginal oscillator. Figure 3 shows the circuit diagram of the marginal oscillator. The low-

transmission loss substrate (MCL-LW-910G, Showa Denko Materials Co., Ltd., Tokyo, Japan) was used as a printed circuit board. Its physical properties were dielectric substrate thickness 0.78 mm, copper laminate thickness 18 μm, relative dielectric constant ε_r 3.3, and dielectric loss tangent $\tan\delta$ 0.002. These properties were used to design (i) the transmission line length, (ii) the oscillation condition at 2.0 GHz on the printed circuit board, and (iii) the ease of processing the substrate. Since weak magnetic coupling was desirable to meet the oscillation conditions, the LGR was placed on the backside of the printed circuit board to distance the LGR from the coupling loop.

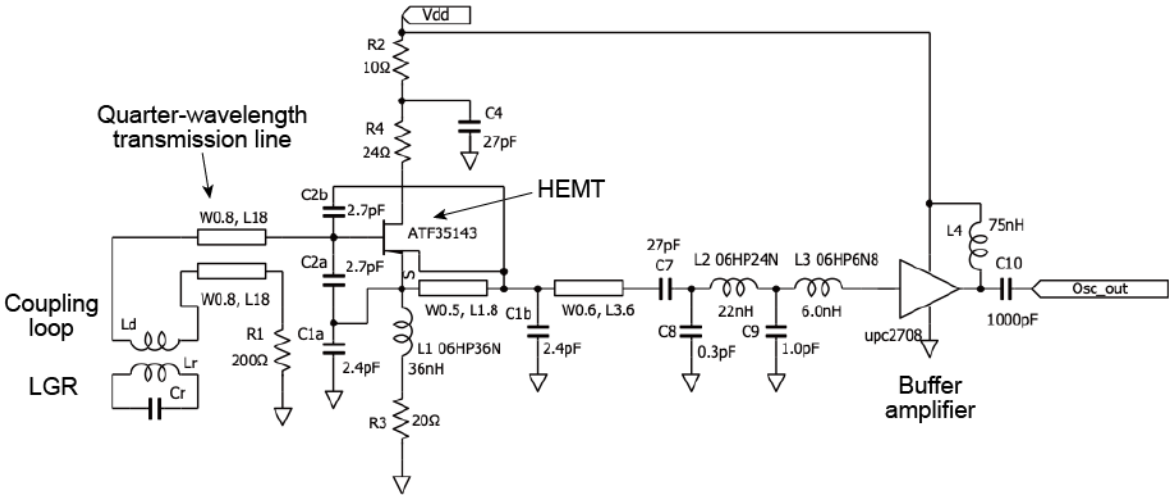

Fig. 3. Circuit diagram of the marginal oscillator. The voltage supply for the oscillator Vdd was 5 V. HEMT (AVAGO ATF35143) and the buffer amplifier (CEL upc2708) were used in the oscillator to monitor the oscillator's output. The current consumption of the oscillator was 56 mA, including the buffer amplifier.

Figure 4A shows a photograph of the implemented marginal oscillator. Figure 4B also shows the backside of the circuit board of the oscillator. The coupling loop's inner diameter was 5.2 mm (the same as the inner diameter of the LGR), and the line

width of the coupling loop was 1.0 mm. The quarter-wavelength transmission line between the coupling loop and the transistor was 18 mm, and the width of the transmission line was 0.8 mm.

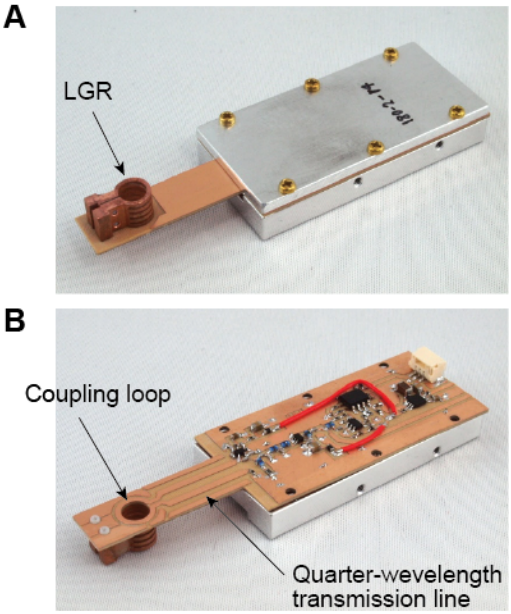

Fig. 4. Implemented marginal oscillator. Photographs of the oscillator and the LGR (A) and the backside of the oscillator circuit (B).

2.4. Spectrometer's Electronics

To demonstrate the lubrication oil measurements, we built two electronics units for the spectrometer in addition to the LGR and the oscillator.

Analog signal processing circuits

The analog signal processing circuits consisted of three circuit boards, each of which functions to demodulate the modulated oscillator output signal, drive the modulation coils, and drive the magnetic field scanning. The details of the analog signal processing circuits are given in the Supplementary Material (Figs. S1–S3).

Power supply and intermediate frequency (IF) circuits

The power supply circuit converted 100 V alternating voltage to 6 V and 9 V direct-current and provided them to the oscillator circuit, the analog signal processing circuit, and the IF circuit. These voltages were further converted to 3.3 V and 5 V on each electronics unit. The microcomputer and the IF circuit performed the phase adjustment for demodulating the ESR signal, the drive signal generation for magnetic field scanning, and the sensor-output signal accumulation. The Bluetooth module circuit and the interface circuit were also implemented on the circuit board.

2.5. Spectrometer Setup

Figure 5A shows the overall spectrometer setup and the user interface on a mobile phone display. The dimensions and weight of the spectrometer were 177 mm x 108 mm x 70 mm (volume 1.3 L) and 1.45 kg. Using an Android mobile phone and Bluetooth interface, the microcomputer controlled the measurement parameters, such as phase adjustment for demodulating the ESR signal, the magnetic field sweep range, and the number of signals accumulated. Moreover, the Android mobile phone displayed the ESR spectrum and the lubrication oil degradation index calculated from the peak-to-peak signal amplitude of the ESR spectrum. Figure 5B shows the spectrometer setup that was enclosed in an aluminum box shown in Fig. 5A. Figures 5C and 5D show the analog signal processing unit and the power supply/IF circuit unit, respectively. As shown in Fig. 5E, the oscillator circuit was placed above the analog signal processing unit. The resonator position on the oscillator’s circuit board was adjusted to the center of the magnet.

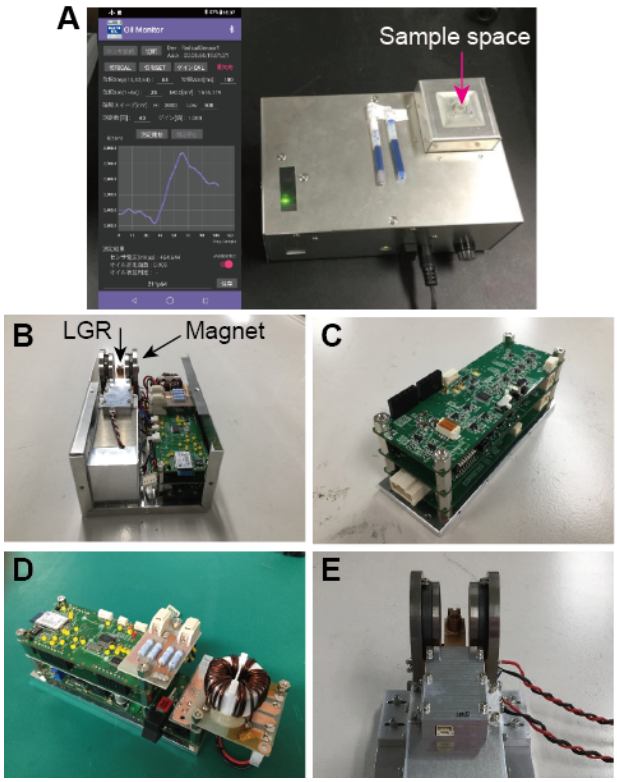

Fig. 5. Prototype spectrometer setup. Photographs of the overall spectrometer and the monitor display of a mobile phone (A), the spectrometer in the enclosure (B), the analog signal processing unit (C), the power supply/IF circuit unit (D), and the alignment of the marginal oscillator and the magnet (E).

2.6. Magnet

The distance between the magnetic pole caps could be reduced to 13.6 mm by narrowing the substrate's width on which the LGR was placed to 10 mm. Figure 6 shows the magnet system using a Ferrite magnet that generated a magnetic field of 68.3 mT at the magnet center. Since the oscillator's target frequency was 2.0 GHz (corresponding magnetic field 71.5 mT), the magnetic field of 68.3 mT was considered to be the lowest magnetic field of the spectrometer. As seen in Fig. 6, the modulation coil was wound inside the pole caps, and the magnetic field sweep coil was wound on the base of the magnetic circuit. The dimensions of the permanent

magnet were 40 mm x 55 mm x 72 mm. Table 1 summarizes the properties of the magnet.

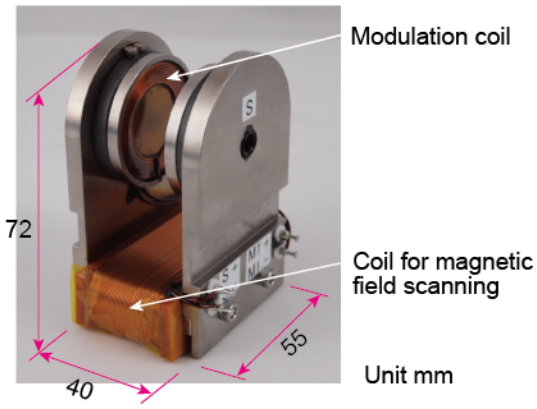

Fig. 6. Photograph of the magnet system. The modulation coils were placed on the surface of the pole caps. The field sweep coil was wound on the base of the magnetic circuit.

Table 1. Properties of the magnet used for the prototype ESR spectrometer.

Distance between pole caps	13.6 mm
Magnetic field strength	68.3 mT
Maximum variation of the magnetic field in the cylindrical space of 10-mm diameter and 6-mm axial length	0.12 mT
Magnetic field sweep range	0 –10 mT by the current 0–1 A
Amplitude of magnetic field modulation	0.58 mT @ 0.5 A
Weight	0.43 kg

2.7. Measurements and Simulation of Microwave Characteristics

Scattering-matrix parameters (S-parameters) of the inductively coupled LGR were measured with a vector network analyzer (E5071C, Keysight Technologies, Santa Rosa, CA). The Q-factor of the oscillator was calculated by the method described in the literature [47]. In the circuit simulation for the Q-factor and the phase characteristics, we used the measured S_{11} parameter for the single-turn loop inductively coupled with the LGR. The phase noise characteristics of the oscillator were measured with a signal source analyzer (E5052B, Keysight Technologies, Santa Rosa, CA). A single-turn loop, called a pick-up coil, connected to a 50-ohm semi-rigid coaxial cable (1.19 mm in diameter, SC-119/50, Coax Corp., Yokohama, Japan) was placed at the center of the LGR to measure an RF magnetic field. The pick-up coil had a mean diameter of 1.29 mm and a wire thickness of 0.287 mm. The RF power generated in the pick-up coil was measured with a vector network analyzer (E5080A, Keysight Technologies, Santa Rosa, CA). Next, the detected RF power was converted to the RF magnetic field B_1 by taking Faraday's law of induction, the complex impedance of the single-turn loop, and the characteristic impedance of the coaxial line into account. Moreover, we used a microwave design tool (Advanced Design System, Keysight Technologies, Santa Rosa, CA) to simulate the characteristics of our marginal oscillator.

2.8. Samples

To test the sensitivity of the spectrometer setup, we prepared known samples by mixing 2,2-diphenyl-1-picrylhydrazyl (DPPH) powder (Sigma-Aldrich, St. Louis, MO) and potassium bromide (KBr) (FUJIFILM Wako Pure Chemical Corp., Osaka, Japan). The samples of DPPH powder were prepared at two concentrations (sample A 3.72×10^{19} spins/L and sample B 4.64×10^{20} spins/L). The lubrication oil sample

was CASTLE DH-2 10W-30 (Toyota Motor Corp., Toyota, Japan). This lubrication oil was used in a truck-type vehicle, a Hino Ranger FD7JPY, and the mileage was 23,770 km. A 50 μL oil sample was placed in a 5.0-mm ESR sample tube and left for 2 hours until it fell to the bottom of the tube.

2.9. ESR Spectroscopy at X-band

An X-band CW-ESR spectrometer (ELEXSYS E500, Bruker Biospin, Germany) was used to prepare the reference samples of DPPH. The number of electron spins was quantified using Xepr software (Bruker Biospin). The measurement parameters of X-band spectroscopy for DPPH samples were as follows: microwave frequency 9.85 GHz, applied microwave power 0.63 mW (RF magnetic field 5.5 μT), magnetic field modulation 0.1 mT at 100 kHz, time constant 30 ms, field sweep duration 3.0 s, and data points 1000/scan. For an oil sample, the measurement conditions were as follows: microwave power 3.17 mW (RF magnetic field 12.4 μT), microwave frequency 9.6 GHz, magnetic field modulation amplitude 0.1 mT at 100 kHz, time constant 30 ms, field sweep duration 3.0 s, number of accumulations 10, and data points 1000/scan. Since the conversion efficiency of the RF magnetic fields for the resonator (Bruker ER4122 SHQE resonator) used for the X-band EPR spectrometer is known to be 0.22 mT/$W^{-1/2}$ at Q = 8355, we roughly estimated the RF magnetic field B_1 from the applied microwave power and this conversion efficiency.

2.10. ESR Spectroscopy at 2 GHz

To demonstrate the monitoring of oil degradation with the prototype spectrometer, the measurement parameters of ESR spectroscopy at 2.0 GHz were as follows: modulation frequency 31.25 kHz, magnetic field modulation 0.4 mT (peak-

to-peak sinusoidal voltage for driving the modulation coil 1.6 V), magnetic field sweep range 71–76 mT, field sweep duration 3.0 s, data points 100/scan, time-constant of lock-in detection 72 ms, and number of accumulations 10. The total measurement time was 30 s. (See section 3.2 for the RF magnetic field B_1 in the LGR.)

3. Results and Discussion

3.1. Resonator Characteristics

Figure 7A shows the Q-factor frequency-dependence of the resonator system in the circuit simulation results, combining the LGR, the coupling loop, and the transmission line. The peak Q-factor was 213 at a frequency of 2.228 GHz for the LGR and the coupling loop (LGR + CL). Two peaks of the Q-factor were observed through inductive coupling. This profile is known as the double-hump response for an inductively coupled resonant system. Figures 7B and 7C show the phase characteristics of the inductively coupled LGR before and after inserting the quarter-wavelength transmission line between the coupling loop and the HEMT. By adding the quarter-wavelength transmission line, the impedance of the LGR was converted from a capacitive value to an inductive value near the resonant peak. The oscillation condition of the oscillator was thus satisfied at 2.085 GHz in this circuit simulation.

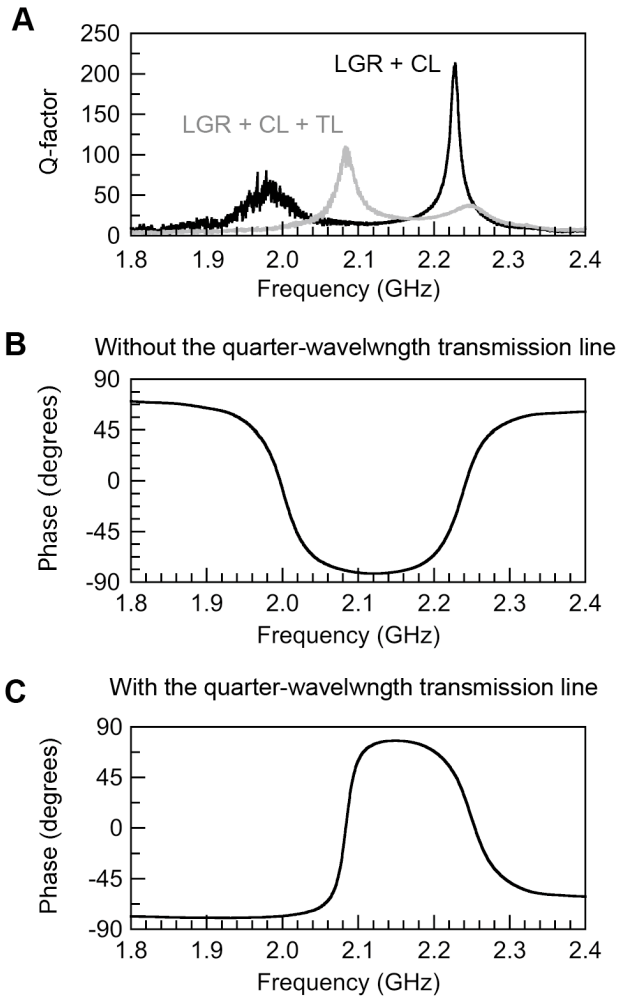

Fig. 7. Microwave characteristics of the LGR, including the coupling loop and the transmission line. (A) Quality factor frequency-dependence calculated at the port of the coupling loop is shown with a black line (LGR + CL). Moreover, quality factor frequency-dependence calculated at the port of the quarter-wavelength transmission line is shown with a gray line (LGR + CL + TL). Phase characteristics at the port of the coupling loop (B) and the quarter-wavelength transmission line (C) correspond to two cases in Fig. 7A. CL denotes the coupling loop, and TL denotes the quarter-wavelength transmission line.

3.2. Oscillator Characteristics

Figure 8A shows the phase noise characteristics of the prototype oscillator. The oscillator's output frequency was 2.09 GHz; the output power for the phase-noise

measurement was 2.4 dBm (1.74 mW). This output power was limited by the linearity of the buffer amplifier (upc2708 in Fig. 3). The phase noise at 100 kHz offset from the carrier frequency was –110 dBc/Hz. Although this phase noise level at 100 kHz offset is larger than those in commercially available voltage-control oscillators and spectrometers, the results in Figs. 7 and 8 verified that our design concept of the oscillator worked adequately.

Figure 8A also shows the simulated phase noise characteristics for the oscillator (gray line). The phase noise was –138 dBc/Hz at 100 kHz offset. This phase noise is 28 dB below the measured phase noise. Such a discrepancy in the phase noise is mainly related to modeling of the HEMT device. Modeling of the device is usually focused on small signal characteristics. However, the HEMT in the oscillator works in the non-linear region and is saturated. In addition, actual HEMT devices have different saturation and high-power characteristics. Overall, the measured phase noise level was much higher than the simulated one. Nevertheless, we used the simulation of the phase noise to optimize the oscillator even if the absolute value of the phase noise does not well agree with the measured characteristics.

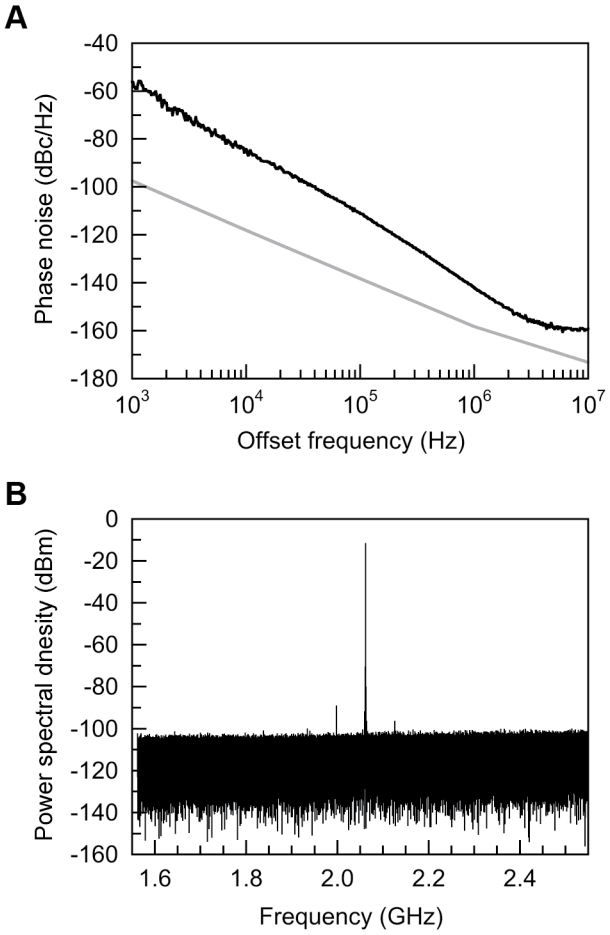

Fig. 8. Measured characteristics of an implemented oscillator. (A) Phase noise characteristics of the oscillator operating at 2.09 GHz. Black and gray lines show the measured and simulated phase noise characteristics, respectively. (B) Power spectral density characteristics of the RF magnetic fields measured with the pick-up coil at the center of the resonator (receiver bandwidth 1 kHz).

Since the oscillator included the LGR in its circuitry, we cannot directly measure the microwave power to the LGR in a conventional manner for a typical reflection-type ESR bridge. Therefore, we directly measured the RF magnetic field in the LGR by using a small pick-up coil. When the pick-up coil was placed in the LGR, the output frequency of the oscillator was slightly shifted from 2.090 GHz to 2.108 GHz. The estimated RF magnetic field B_1 at the center of the LGR was 27 μT (peak amplitude), which was converted from the detected RF power. In this estimation, the

loading effect in the oscillator due to a pick-up coil was neglected because we could not measure the decrease in the Q-factor of the LGR directly when the oscillator was operating. Therefore, our estimation of the RF magnetic field may have some errors due to the loading effect and the interference in the RF magnetic field with a semi-rigid coaxial cable.

Moreover, Fig. 8B shows the power spectral density characteristics (1.55 to 2.55 GHz) of the RF magnetic fields at the center of the LGR. The RF magnetic fields were detected with the pick-up coil at the center of the LGR. The power spectral density (noise floor) in this frequency band was flat. The detected oscillation signal and the power spectral density level of the noise floor were approximately –11.7 dBm and –102 dBm (90 dB below the oscillation signal level) with a receiver bandwidth of 1 kHz. Small peaks (–89.2 and –96.5 dBm) of the sidebands are visible at ±64 MHz from the oscillation frequency. These sidebands mean that the oscillation signal is slightly modulated in amplitude. However, we concluded that the noise of the oscillation voltage is small enough in our oscillator and the RF magnetic fields based on the power spectral density characteristics.

3.3. ESR measurements of DPPH and oil samples

To evaluate the signal sensitivity of the prototype ESR spectrometer, we measured DPPH samples. Two DPPH powder samples (sample A 3.72 x 10^{19} spins/L and sample B 4.64 x 10^{20} spins/L) were prepared to mimic the radical concentration in automobile lubrication oil. The sample volume in the LGR was 75 μL. This volume was calculated from the LGR height (6.0 mm) and the inner diameter of the sample tube (4.0 mm). Figure 9 shows the measured ESR spectra for two DPPH samples at 2.0 GHz. The peak-to-peak ESR signal amplitudes for sample A

(Fig. 9A) and sample B (Fig. 9B) were 48.6 μV and 410 μV, respectively. The signal sensitivity was calculated to be 5.7 x 10^{13} spins/μV for sample A and 8.5 x 10^{13} spins/μV for sample B, with a total acquisition time of 30 s. While there is a slight discrepancy in the detection sensitivity, the signal sensitivity of the prototype compact ESR spectrometer was clarified in this measurement.

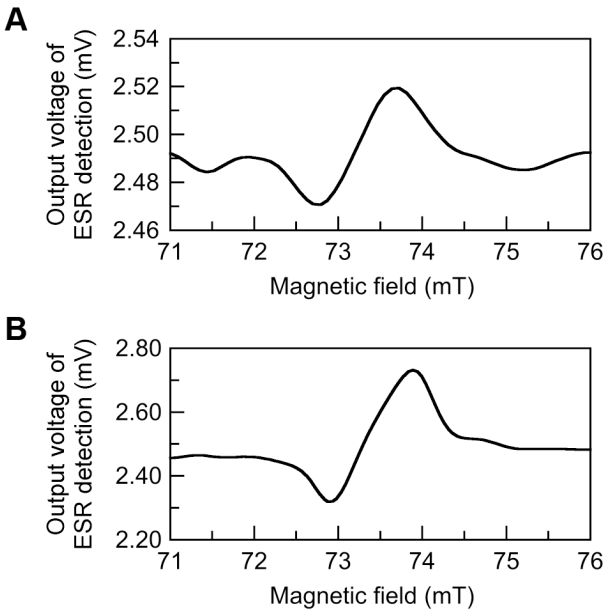

Fig. 9. ESR spectra of the DPPH samples measured at 2.0 GHz. (A) Sample A at a concentration of 3.72×10^{19} spins/L and (B) sample B at a concentration of 4.64×10^{20} spins/L. Since the sample volume of the LGR was 75 μL, 2.79 x 10^{15} spins (A) and 3.48 x 10^{16} spins (B) were measured in the DPPH samples.

The measured peak-to-peak linewidth of the ESR spectrum of DPPH in Fig. 9 was much broader than the typical linewidth of DPPH (0.29 mT, measured by X-band ESR spectroscopy). This linewidth broadening is thought to be due to (i) over-modulation (modulation amplitude 0.4 mT), (ii) slow response of phase-sensitive detection, and (iii) inhomogeneity of the magnetic field (see Table 1). Since the field

inhomogeneity is smaller than the intrinsic linewidth of DPPH, the first two factors mainly broadened the recorded spectral lineshape of the DPPH samples.

In addition to the modulation amplitude, power saturation of the spin system in a sample is another consideration for ESR spectroscopy. Our marginal oscillator spectrometer had limited capability for controlling the RF signal level. Therefore, we did not perform a power saturation test for the samples to optimize ESR measurements.

In this application of monitoring lubrication oil degradation, we thought that the electromagnetic noise from the environment and the vibration of the spectrometer and the sample would be higher than in a conventional laboratory setup. Therefore, we applied a slow response (lower cut-off frequency) for filtering in phase-sensitive detection to suppress the noise on the spectral baseline. The ESR spectral lineshape might have some distortions as a result (see Fig. 9). However, even a rough readout of the peak-to-peak amplitude of the ESR signal is suitable for our application.

We further measured the used oil sample to demonstrate the ESR measurements of free radicals in automobile lubrication oil (23,770 km mileage). Figure 10A shows the ESR spectrum of the oil sample (50 μL) obtained as a reference using X-band ESR spectroscopy. The concentration of free radicals in the oil sample was determined to be 8.3×10^{19} spins/L by X-band ESR spectroscopy. Figure 10B shows the ESR spectrum of the used oil sample with the prototype ESR spectrometer. The peak-to-peak signal amplitude and linewidth were 80.7 μV and 1.01 mT, respectively. The measured data for unused oil are also shown in Fig. 10B. The lack of an ESR absorption peak for unused oil demonstrates that ESR spectral detection occurs when the absorption signal exists.

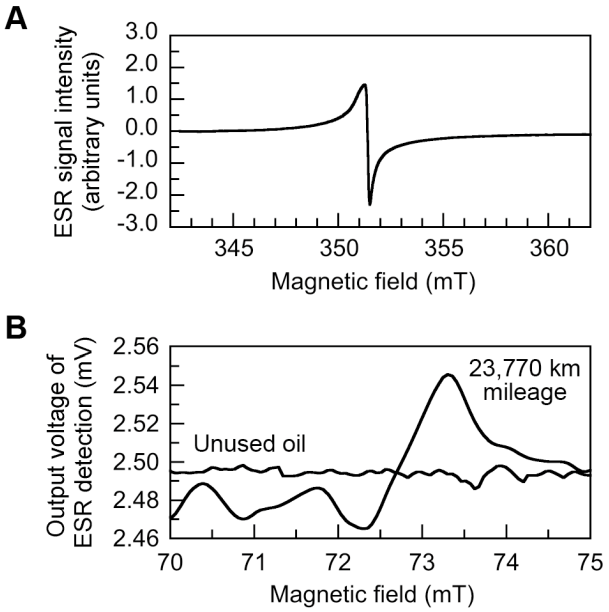

Fig. 10. ESR spectra of lubrication oil samples. (A) Reference X-band ESR spectrum for the degraded oil sample (23,770 km mileage), (B) ESR spectra of unused and used oil samples measured with the 2.0-GHz prototype spectrometer.

For the spectral baseline of unused oil in Fig. 10B, the standard deviation *SD* was 2.17 μV. When we define 2 *SD* as the spectral baseline noise level, the SNR of the ESR spectrum is given as the ratio of the peak-to-peak signal intensity to the noise level. The SNR of the spectrum for the used oil (23,770 km) was 37 as the best-case scenario.

Fluctuation of the spectral data in 70 to 72 mT is seen in Fig. 10B; however, it was not reproducible. This fluctuation is thus not part of the ESR signal and degrades the SNR of the spectrum. However, the ESR-based monitoring of lubrication oil degradation will detect the peak-to-peak amplitude of the spectrum as the monitor output. Therefore, baseline fluctuation is less problematic for the monitoring of lubrication oil degradation. Although we do not present the systematic investigation of the SNR degradation due to this baseline fluctuation, which appeared only

temporarily, an in-depth investigation of the SNR of the spectrum would be useful for future improvement of our compact spectrometer. The following discussion is based on the best-case scenario of the SNR of the spectrum.

Suppose SNR = 2 to be the EPR spectrum detection limit for the degradation of lubrication oil. The oil degradation detection limit in terms of mileage was estimated to be approximately 1300 km from the obtained SNR because the EPR signal intensity has been shown to be proportional to the mileage of the lubrication oil sample [25]. The spin concentration at the detection limit was also estimated to be 8.3×10^{19} spins/L / (37 / 2) = 4.5×10^{18} spins/L. The corresponding number of spins in the 50 μL sample was determined to be 2.3×10^{14} spins. As a result, the detection limit of the spectrometer was 2.3×10^{14} spins under the condition of a 1.0 mT linewidth and an acquisition time of 30 s at B_1 = 27 mT.

The spin concentration detection limit was on the order of 10^{18} spins/L and met the detection sensitivity requirement, point (ii) of the required features. The prototype compact spectrometer had a detection limit of 2.3×10^{14} spins in the oil sample (50 μL). This sensitivity was reasonably high for assessing the degradation of lubrication oil. As a result, we have successfully designed and developed a compact ESR spectrometer for monitoring oil degradation.

Marginal oscillator spectrometers were previously investigated in nuclear magnetic resonance (NMR) and ESR. Donnally and Sanders reported a simple transistor marginal oscillator for magnetic resonance in 1960. They stated that “the signal-to-noise is about half that for a Pound-Watkins-Knight circuit.” [48]. Moreover, Howling analyzed the signal and noise of the marginal oscillator spectrometer and verified the derived results with the NMR spectra of ^{63}Cu powder measured at 9 MHz [49]. Adler, Senturia, and Hewes also reported the noise sources and the sensitivity

of marginal oscillator spectrometers [50]. In the literature [50], 1/*f* noise and the mixer noise were examined in addition to the signal output voltage. Furthermore, Rahf developed a marginal resonator for NMR spectroscopy (1.5 to 15.3 T with a frequency of 60 to 110 MHz) and reported the SNRs of NMR spectroscopy for several nuclei [51]. In addition, Kemper and Bowers analyzed bridge circuit and marginal oscillator detectors; however, they did not present an experimental comparison of the two detection schemes [52]. A sensitivity comparison of our marginal oscillator spectrometer and the standard reflection-type bridge spectrometer will be helpful for further investigations. Since we used the LGR, which has a relatively lower *Q*-factor, in the marginal oscillator, this resonator choice might degrade the oscillator's phase noise and impact the sensitivity of the spectrometer. Noise sources such as the oscillator's phase noise and thermal noise of the modern marginal oscillator reported here can be analyzed by considering early works.

Since this article focused on the development of a 2.0-GHz compact ESR spectrometer, we did not show much spectral data for lubrication oil degradation. The dependence of free radical generation in lubrication oil with various mileages has been reported elsewhere [25]. However, Fig. 10B clearly shows that free radical generation is a marker of lubrication oil degradation. Our prototype spectrometer had an enclosure volume of 1.3 L and a weight of 1.45 kg, including the magnet. These achievements meet our aim of developing a compact spectrometer that can be used in daily service in the automobile industry. The prototype spectrometer is much smaller than the Micro-ESR spectrometer reported in 2010 [42]. Moreover, its weight (1.45 kg) is much less than those of commercial X-band ESR spectrometers such as the Bruker microESR (10 kg), Bruker Magnettech ESR5000 (45 kg), and Adani APINSCAN X (45 kg). Also, the user interface was built on a commonly used Android

mobile phone. These advances have enabled ESR spectroscopy for monitoring lubrication oil degradation.

4. Conclusion

In this work, a marginal oscillator contributed to a simple microwave circuitry of the spectrometer. Furthermore, the prototype spectrometer achieved a detection sensitivity of 2.3 x 10^{14} spins under the condition of a 1.0 mT linewidth and an acquisition time of 30 s. This sensitivity limitation corresponds to a spin concentration of 4.5 x 10^{18} spins/L for automobile lubrication oil. In addition to the ESR detection sensitivity, compactness and low weight of the spectrometer were realized. These advances may contribute to the excellent maintenance of engines with the right balance between automobile engine protection and reducing oil waste in the future.

Acknowledgments

The authors are grateful to Prof. Gareth R. Eaton, University of Denver, CO, USA, for his helpful suggestions on the literature of EPR detection using marginal oscillator spectrometers. This work was supported by MIRISE Technologies Corporation.

Appendix

Supplementary Materials: Schematic diagrams of the analog signal processing circuits are shown in Figs. S1, S2, and S3.

Author contributions

Fan Cheng: Methodology, Investigation, Visualization, Writing- Original draft preparation

Takayuki Shibata: Conceptualization, Methodology, Investigation, Visualization, Project administration, Writing- Reviewing and Editing

Yoshifumi Aoki: Investigation

Hiroshi Hirata: Validation, Visualization, Writing- Original draft preparation, Writing- Reviewing and Editing

References

[1] US Department of Energy, Used Oil Management and Beneficial Reuse Options to Address Section 1: Energy Savings from Lubricating Oil Public Law 115-345, Report to Congress, 2020 (Chapter III). https://www.energy.gov/fe/downloads/used-oil-management-and-beneficial-reuse-report-congress (accessed 2021.06.05).

[2] J. Zhu, D. He, E. Bechhoefer, Survey of lubrication oil condition monitoring, diagnostics, and prognostics techniques and systems, J. Chem. Sci. Technol. 2 (2013) 100–115.

[3] J. Zhu, Online industrial lubrication oil health condition monitoring, diagnosis and prognostics, Ph.D. Thesis, University of Illinois at Chicago, 2013

[4] I.I. Khandaker, E. Glavas, G.R. Jones, A fibre-optic oil condition monitor based on chromatic modulation, Meas. Sci. Technol. 4 (1993) 608–613. https://doi.org/10.1088/0957-0233/4/5/011

[5] M. Scherer, M. Arndt, P. Bertrand, B. Jakoby, Fluid condition monitoring sensors for diesel engine control, in: Proceedings of IEEE Sensors 2004 (2004) 459–462. https://doi.org/10.1109/ICSENS.2004.1426199

[6] S. Kumar, P.S. Mukherjee, N.M. Mishra, Online condition monitoring of engine oil, Ind. Lubr. Tribol 57 (2005) 260-267. https://doi.org/10.1108/00368790510622362

[7] M. Al-Ghouti, L. Al-Atoum, Virgin and recycled engine oil differentiation: a spectroscopic study, J. Environ. Manage. 90 (2009) 187–195. https://doi.org/10.1016/j.jenvman.2007.08.018

[8] A. Agoston, C. Ötsch, J. Zhuravleva, B. Jakoby, An IR-absorption sensor system for the determination of engine oil deterioration, in: Proceedings of IEEE Sensors 2004 (2004) 463–466. https://doi.org/10.1109/ICSENS.2004.1426200

[9] H. Shinde, A. Bewoor, Analyzing the relationship between the deterioration of engine oil in terms of change in viscosity, conductivity and transmittance, in: Proceedings of 2017 International Conference on Advances in Mechanical, Industrial, Automation and Management Systems (AMIAMS) (2017) 36–41. https://doi.org/10.1109/AMIAMS.2017.8069185

[10] A. Basu, A. Berndorfer, C. Buelna, J. Campbell, K. Ismail, Y. Lin, L. Rodriguez, S.S. Wang, Smart sensing of oil degradation and oil level measurements in gasoline engines, SAE Tech. Pap. (2000) 2000-01-1366. https://doi.org/10.4271/2000-01-1366

[11] S. Raadnui, S. Kleesuwan, Low-cost condition monitoring sensor for used oil analysis, Wear 259 (2005) 1502–1506. https://doi.org/10.1016/j.wear.2004.11.009

[12] V. Balashanmugam, G. Devaradjane, Development of dielectric sensor to monitor the engine lubricating oil degradation, Therm. Sci. 20 (Suppl. 4) (2016) 1061–1069. https://doi.org/10.2298/TSCI16S4061B

[13] C. Chiang, Y. Huang, A semicylindrical capacitive sensor with interface circuit used for flow rate measurement, IEEE Sens. J. 6 (2006) 1564–1570. https://doi.org/10.1109/JSEN.2006.883847

[14] H. Shinde, A. Bewoor, Capacitive sensor for engine oil deterioration measurement, AIP Conf. Proc. 1943 (2018) 020099. https://doi.org/10.1063/1.5029675

[15] J.W. Bennett, L. Matsiev, M. Uhrich, O. Kolosov, Z. Bryning, R. Lattin, New solid state oil condition sensor for real time engine oil condition monitoring, SAE Tech. Pap. (2006) 2006-01-1324. https://doi.org/10.4271/2006-01-1324

[16] M. Kasai, N. Yoshimura, K. Watanabe, Evaluation of engine oil deterioration using a comb-shaped electrode, SAE Tech. Pap. (2016) 2016-01-2317. https://doi.org/10.4271/2016-01-2317

[17] A. Agoston, C. Ötsch, B. Jakoby, Viscosity sensors for engine oil condition monitoring: Application and interpretation of results, Sens. Actuator A Phys. 121, (2005) 327–332.

[18] B. Jakoby, M. Scherer, M. Buskies, H. Eisenschmid, An automotive engine oil viscosity sensor, IEEE Sens. J. 3 (2003) 562–568. https://doi.org/10.1109/JSEN.2003.817164

[19] S. Yunus, A.A. Rashid, S.A. Latip, N.R. Abdullah, M.A. Ahmad, A.H. Abdullah, Comparative study of used and unused engine oil (Perodua Genuine and Castrol Magnatec Oil) based on Property Analysis Basis, Procedia Eng. 68 (2013) 326–330. https://doi.org/10.1016/j.proeng.2013.12.187

[20] C. Zhang, H. George, B. Soukup, R. Kornbrekke, F.P. Boyle, S.A. Goodlive, Chemical sensor development for measuring soot caused lubricant oil thickening, in: Proceedings of the 2004 IEEE International Frequency Control Symposium and Exposition (2004) 200–205. https://doi.org/10.1109/FREQ.2004.1418453

[21] A. Basu, W. Ruona, G. Zawacki, A. Gangopadhyay, D. Scholl, J. Visser, H. Dobrinski, M. Doebrich, Development and Testing of an Innovative Oil Condition Sensor, SAE Int. J. Engines 2 (2009) 1327-1334. https://doi.org/10.4271/2009-01-1466

[22] J. Milpied, M. Uhrich, B. Patissier, L. Bernasconi, Applications of tuning fork resonators for engine oil, fuel, biodiesel fuel and urea quality monitoring, SAE Int. J. Fuels Lubr. 2 (2010) 45-53. https://doi.org/10.4271/2009-01-2639

[23] M. Diaby, M. Sablier, A. Le Negrate, M. El Fassi, J. Bocquet, Understanding carbonaceous deposit formation resulting from engine oil degradation, Carbon 47 (2009) 355–366. https://doi.org/10.1016/j.carbon.2008.10.014

[24] C.-I Chen, S.M. Hsu, A chemical kinetics model to predict lubricant performance in a diesel engine. Part I: simulation methodology, Tribol. Lett. 14 (2003) 83–90. https://doi.org/10.1023/A:1021748002697

[25] F. Cheng, T. Shibata, Y. Aoki, H. Hirata, Development of an oil degradation sensor based on detection of free radicals, SAE Tech. Pap. (2019) 2019-01-2299. https://doi.org/10.4271/2019-01-2299

[26] W.M. Walsh Jr., L.W. Rupp Jr., A self-detecting microwave marginal oscillator, Rev. Sci. Instrum. 42 (1971) 468–470. https://doi.org/10.1063/1.1685132

[27] L.W. Rupp Jr., W.M. Walsh Jr., A. Steinfeld, A simplified microwave frequency electron spin resonance spectrometer, Am. J. Phys. 38 (1970) 238–242. https://doi.org/10.1119/1.1976293

[28] W.M. Walsh Jr., L.W. Rupp Jr., A microwave frequency marginal oscillator for electron spin resonance, Rev. Sci. Instrum. 41 (1970) 1316–1318. https://doi.org/10.1063/1.1684804

[29] F. Momo, A. Sotgiu, Cavity stabilised Impatt oscillator for ESR spectroscopy, J. Phys. E: Sci. Instrum. 14 (1981) 339–344. https://doi.org/10.1088/0022-3735/14/3/018

[30] K.W. Pontinen, J.P. Cruts, A.B. Denison, Gun-effect diode EPR spectrometer, J. Magn. Reson. 6 (1972) 371–375. https://doi.org/10.1016/0022-2364(72)90110-2

[31] Y.V. Bogachev, M.N. Knyazev, A.V. Nikitina, Features of development and applications of compact EPR analyzers, Appl. Magn. Reson. 50 (2019) 605–617. https://doi.org/10.1007/s00723-018-1088-9

[32] R.D. Hogg, A low cost X-Band IMPATT diode marginal oscillator for EPR, Am. J. Phys. 41 (1973) 224–229. https://doi.org/10.1119/1.1987180

[33] G. Boero, M. Bouterfas, C. Massin, F. Vincent, P.-A. Besse, R. S. Popovic, A. Schweiger, Electron-spin resonance probe based on a 100 μm planar microcoil, Rev. Sci. Instrum. 74 (2003) 4794-4798. https://doi.org/10.1063/1.1621064

[34] T. Yalcin, G. Boero, Single-chip detector for electron spin resonance spectroscopy, Rev. Sci. Instrum. 79 (2008) 094105. https://doi.org/10.1063/1.2969657

[35] J. Handwerker, B. Schlecker, U. Wachter, P. Radermacher, M. Ortmanns, J. Anders, A 14GHz Battery-operated point–of-care ESR spectrometer based on a 0.13μm CMOS ASIC, 2016 IEEE International Solid-State Circuits Conference Digest Tech. (2016) 476–477. https://doi.org/10.1109/ISSCC.2016.7418114

[36] A. Chu, B. Schlecker, K. Lips, M. Ortmanns, J. Anders, An 8-channel 13GHz ESR-on-a-chip injection-locked VCO-array achieving 200μM-concentration sensitivity, 2018 IEEE International Solid-State Circuits Conf. Digest Tech. (2018) 354–356. https://doi.org/10.1109/ISSCC.2018.8310330

[37] A.V. Matheoud, G. Gualco, M. Jeong, I. Zivkovic, J. Brugger, H. M. Rønnow, J. Anders, G. Boero, Single-chip electron spin resonance detectors operating at

50GHz, 92GHz, and 146GHz, J. Magn. Reson. 278 (2017) 113–121. https://doi.org/10.1016/j.jmr.2017.03.013

[38] A.V. Matheoud, N. Sahin, G. Boero, A single chip electron spin resonance detector based on single high electron mobility transistor, J. Magn. Reson. 294 (2018) 59–70. https://doi.org/10.1016/j.jmr.2018.07.002

[39] H. Sato-Akaba, M.C. Emoto, H. Hirata, H.G. Fujii, Design and testing of a 750 MHz CW-EPR digital console for small animal, J. Magn. Reson. 284 (2017) 48–58. https://doi.org/10.1016/j.jmr.2017.09.008

[40] H. Sato-Akaba, M. Tseytlin, Development of an L-band rapid scan EPR digital console, J. Magn. Reson. 304 (2019) 42–52. https://doi.org/10.1016/j.jmr.2019.05.003

[41] J. Kozioł, P. Rajda, R. Rumian, T. Oleś, P. Budzioch, R.J. Gurbiel, W. Froncisz, Continuous wave electron paramagnetic resonance L-band spectrometer with direct digitalization using time-locked subsampling, J. Magn. Reson. 322 (2021) 106870. https://doi.org/10.1016/j.jmr.2020.106870

[42] C.J. White, C.T. Elliott, J.R. White, Micro-Electron Spin Resonance (EPR/ESR) spectroscopy, Proc. SPIE 7680 (2010) 76800O. https://doi.org/10.1117/12.849682

[43] G.A. Rinard, R.W. Quine, J.R. Harbridge, R. Song, G.R. Eaton, S.S. Eaton, Frequency dependence of EPR signal-to-noise, J. Magn. Reson. 140 (1999) 218–227. https://doi.org/10.1006/jmre.1999.1798

[44] W.N. Hardy, L.A. Whitehead, Split-ring resonator for use in magnetic resonance from 200–2000 MHz, Rev. Sci. Instrum. 52 (1981) 213–216. http://dx.doi.org/10.1063/1.1136574

[45] W. Froncisz, J.S. Hyde, The loop-gap resonator: A new microwave lumped circuit ESR sample structure, J. Magn. Reson. 47 (1982) 515–521. https://doi.org/10.1016/0022-2364(82)90221-9

[46] I.M. Gottlieb, Practical Oscillator Handbook, Newnes, Oxford, 1997 (Chap. 4).

[47] T. Ohira, K. Araki, Active Q-factor and equilibrium stability formulation for sinusoidal oscillators, IEEE Trans. Circuits Syst Part II Express Briefs 54 (2007) 810–814. https://doi.org/10.1109/TCSII.2007.899952

[48] B. Donnally, T.M. Sanders, Jr., Simple transistor marginal oscillator for magnetic resonance, Rev. Sci. Instrum. 31 (1960) 977–978. https://doi.org/10.1063/1.1717122

[49] D.H. Howling, Signal and noise characteristics of the PKW marginal oscillator spectrometer, Rev. Sci. Instrum. 36 (1965) 660–667. https://doi.org/10.1063/1.1719659

[50] M.S. Adler, S.D. Senturia, C.R. Hewes, Sensitivity of marginal oscillator spectrometers, Rev. Sci. Instrum. 42 (1971) 704–712. https://doi.org/10.1063/1.1685206

[51] L. Rahf, New sensitive marginal oscillator, Rev. Sci. Instrum. 52 (1981) 1361-1363. https://doi.org/10.1063/1.1136772

[52] P.R. Kemper, M.T. Bowers, Toward a frequency scanning marginal oscillator, in: H. Hartmann, K.-P. Wanczek (eds.), Lecture Notes in Chemistry, Volume 31, Ion Cyclotron Resonance Spectrometry II, Springer-Verlag, Berlin, 1982, pp. 326–330. https://doi.org/10.1007/978-3-642-50207-1_19